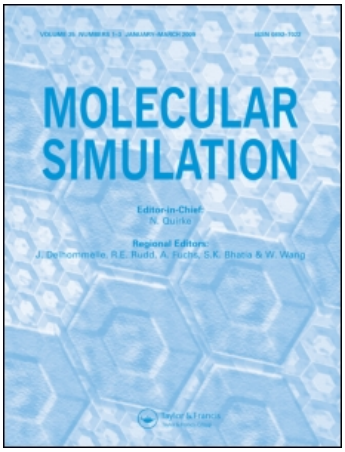

Molecular Simulation
Publication details, including instructions for authors and subscription information:
http://www.informaworld.com/smpp/title~content=t713644482

Computer simulations of two dimensional gold nanoparticle arrays: the influence of core geometry

Kafui Tay[a]; Fernando Bresme[a]
[a] Department of Chemistry, Imperial College London, London, United Kingdom

To cite this Article Tay, Kafui and Bresme, Fernando(2005) 'Computer simulations of two dimensional gold nanoparticle arrays: the influence of core geometry', Molecular Simulation, 31: 6, 515 — 526
To link to this Article: DOI: 10.1080/08927020500035879
URL: http://dx.doi.org/10.1080/08927020500035879

Molecular Simulation, Vol. 31, No. 6-7, 15 May – 30 May 2005, 515–526

Taylor & Francis
Taylor & Francis Group

Computer simulations of two dimensional gold nanoparticle arrays: the influence of core geometry

KAFUI TAY and FERNANDO BRESME*

Department of Chemistry, Imperial College London, Exhibition Road, London SW7 2AZ, United Kingdom

(Received December 2004; in final form December 2004)

We report molecular dynamics computer simulations of gold passivated nanoparticles and gold nanoparticle arrays. We investigate Au_{140} butane and dodecanethiol passivated clusters. In particular we analyse the effect that the metal core structure has on the interparticle forces and the self assembly of small nanoparticle arrays. We find that the core geometry has very little influence on the intermolecular forces, except for interparticle distances close to contact. Also the core geometry has little influence in determining the structure of the molecular arrays. The structure of the arrays is very rich, from open structures, similar to the ones appearing in limited diffusion process, to compact structures, whose symmetry depends on the chain length of the surfactants. We discuss our results with reference to recent experiments on nanoparticle arrays.

Keywords: Gold passivated nanoparticles; Gold nanoparticle arrays; Potential of mean force; Surfactants

1. Introduction

Gold nanoparticles have been the subject of a large number of studies. Metal nanoparticles exhibit properties that significantly differ from those of the bulk crystals [1]. A manifestation of these differences are the electronic properties of nanoparticles, which strongly depend on particle size, interparticle distances and also on the nature of passivating molecules. Also the wetting properties of nanoparticles exhibit a strong dependence with particle size. Recent theoretical studies have illustrated this idea using simplified models of nanoparticles adsorbed at interfaces and dispersed in bulk fluids [2–5]. In addition, particle shape is an important variable determining the stability of nanoparticles at interfaces. We have shown recently that the interplay of shape and line tension can result in a new mechanism that determines the surface activity of nanoparticles at interfaces [6].

Experiments on nanoparticles adsorbed at the water–air interface, have shown that nanoparticles can form rather complex structures [7]. The origin of the interparticle forces determining these structures is still an outstanding question in colloidal science. It is clear that the traditional DLVO theory cannot be applied to explain the interactions in these systems, which in some cases, might consist of neutral particles. Indeed even in the case of charged systems, the DLVO theory is expected to fail when interparticle distances are very small, since the non-local dielectric response of water is neglected (see for instance Ref. [8] for a discussion of a related issue in the context of thin bilayer films). Consequently non-DLVO interactions have been put forward to explain the structure of self assembled nanoparticle arrays. One of these interactions has its origin on the interpretation of surfactants pertaining to different particles, which could lead two an anisotropic interaction between nanoparticles [12].

Recent experiments on silver passivated nanocrystals, have reported the formation of highly oriented molecular arrays [13]. The orientational order has been interpreted as due to the correlation between facets of neighbouring nanocrystals. According to this, the formation of highly oriented structures is connected to the structure of the nanocrystal core. Similar experiments using gold nanoparticles do not seem to agree on the existence of orientational correlations. Thus, some experiments suggest that the symmetry of the superlattices resulting from nanoparticle self assembly depends on the geometry of the nanoparticle core [14], whereas others [15], do not find evidence of a preferred orientation. It is important to recall that nanocrystal orientation might be of importance

*Corresponding author. E-mail: f.bresme@imperial.ac.uk

Molecular Simulation
ISSN 0892-7022 print/ISSN 1029-0435 online © 2005 Taylor & Francis Group Ltd
http://www.tandf.co.uk/journals
DOI: 10.1080/08927020500035879

in electronic transport processes, for instance electron tunnelling, and therefore it is relevant to the design of optimal molecular electronic devices. Consequently, the investigation of questions concerning nanoparticle orientation is of importance for the design of nanomaterials.

Computer simulations represent an ideal tool to analyse intricate self assembled structures, and provide an unambiguous microscopic image of the conformation of the coating surfactant layers as well as the orientation of the nanocrystal cores. Landman and coworkers [10,11,18] have pioneered the modelling studies of gold nanoparticles and three dimensional nanoparticle arrays. To the best of our knowledge, there are no previous simulation studies discussing the effect of core geometry on the interparticle forces or the structure of two dimensional arrays.

In this paper, we investigate using molecular dynamics simulations, gold nanoparticles passivated by thiol-alkane hydrocarbon chains of different lengths. We consider as a starting point a relatively small gold nanocluster with core size, Au_{140}, passivated with butanethiol and dodecanethiol surfactants. Our aim is to investigate the influence of the nanoparticle core geometry in determining (1) the nano-particle shape, (2) the interparticle interactions and (3) the two dimensional structure of self assembled nanoparticle arrays. With this aim we consider both realistic core geometries and also spherically averaged cores.

The paper is organised as follows. In section 2, we discuss the model and simulation methodology. A discussion of the dependence of surfactant structure, mean force potentials and nanoparticle assemblies structure on core geometry follows. A final section with our main conclusions and final remarks closes the paper.

2. Model and methodology

The structure and thermodynamic properties of alkanethiol passivated nanoparticles were investigated using molecular dynamics computer simulations. Two different models have been employed to investigate the significance of the core geometry. Firstly, a detailed model in which the metallic, crystalline core is explicitly considered; and secondly, a simpler, computationally less expensive model in which the crystalline core is modelled as a single sphere.

2.1 Realistic gold core nanoparticle

The realistic gold core was modelled within a truncated octahedral motif consisting of a face centred cubic lattice of 140 gold atoms, see (figure 1). Experimental findings have shown the existence of an energetically optimal sequence of gold nanocrystal structures, of which the Au_{140} nanocrystallite is a member. Theoretical calculations have determined that these structures are characterised by face-centred cubic lattices, possess truncated octahedral morphologies, and present good stability [16]. We have checked this last point with simulations of the bare gold nanocrystal, using the many body embedded atom Sutton–Chen potential parameterised for gold [20,21].

$$U_i(r) = \varepsilon\left[\left(\frac{a}{r}\right)^n - \left(\frac{C}{2}\right)\sqrt{p_i}\right]^n, \quad p_i = \sum\left(\frac{a}{r_{ij}}\right) \qquad (1)$$

The parameters ε, a and C are determined by equilibrium lattice parameters and lattice energies. The exponent pairs, n and m are fitted to elastic constants. For gold, $\varepsilon = 9.383265\,\mathrm{kJ/mol}$, $a = 4.080\,\text{Å}$, $n = 10.0$, $m = 8.0$ and

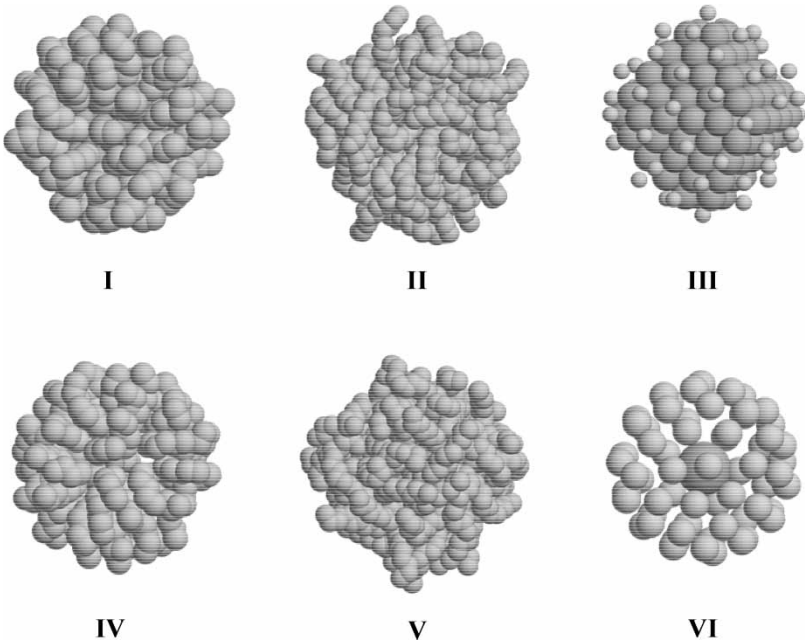

Figure 1. Top: butanethiol (I) and dodecanethiol (II) passivated nanoparticles with Au_{140} crystalline core surrounded by 62 adsorbed sulphur pseudoatoms (III). Bottom: model butanethiol (IV) and dodecanethiol (V) passivated nanoparticles with spherically averaged core surrounded by 62 adsorbed sulphur pseudoatoms (VI).

$C = 34.408$. The melting temperature predicted by the Sutton–Chen model for bulk gold is lower than the experimental value. This does not seem to affect the stability of the small Au_{140} cluster, which was found to be stable at 300 K.

The thiol–gold (SH–Au) interaction was approximated as a non-bonded m–n potential, with parameters compatible with the thiol–gold bonding interaction [22]. The m–n potential is defined as [24],

$$U(r) = \frac{E_0}{n-m}\left[m\left(\frac{r_0}{r}\right)^n - n\left(\frac{r_0}{r}\right)^m\right] \quad (2)$$

where $E_0 = 38.6\,\text{kJ/mol}$, $n = 8$, $m = 4$ and $r_0 = 2.9\,\text{Å}$. The strength of the interaction necessary to replicate the chemical bond often results in unrealistic interactions at intermediate distances (i.e. 6 Å onwards) when simulating systems of more than one nanoparticle. In such cases sulphur pseudoatoms can interact strongly with adjacent nanocrystals. To model the thiol–gold interaction we have used a switched and shifted version of the m–n potential [24]. This potential smoothly converges to zero at a given cutoff distance (in this case, $r_c = 6.2\,\text{Å}$), avoiding any unrealistic interactions. It has been previously reported that the strength of the thiol–gold interaction can result in the penetration and hence disruption of the crystalline core by the sulphur pseudoatoms [17]. Increasing the gold–gold Sutton–Chen interaction by a factor of 5 was found to preserve the morphology and crystallinity of the gold core.

The alkanethiol passivating chains were modelled using united atom potentials, i.e. the CH_2 and CH_3 were represented as pseudoatoms. The alkanethiol intra-molecular interactions were modelled using constraints for the bonds, harmonic potentials for the angular degrees of freedom,

$$U_{\text{angle}}(\theta) = \frac{1}{2}k(\theta - \theta_0)^2 \quad (3)$$

and dihedral angle potentials for the torsional interactions,

$$U_{\text{dihedral}}(\phi) = \frac{1}{2}a_1(1 + \cos(\phi)) + \frac{1}{2}a_2(1 - \cos(2\phi)) + \frac{1}{2}a_3(1 + \cos(3\phi)) \quad (4)$$

Table 1. Surfactant intramolecular interactions [17].

Interacting groups	*Parameters*
Rigid bond CH_3–CH_2	1.54
Rigid bond CH_2–CH_2	1.54
Rigid bond CH_2–SH	1.82
Harmonic angle CH_2–CH_2–CH_3	$k = 519.73$
	$\theta_0 = 114.4$
Harmonic angle CH_2–CH_2–SH	$k = 519.73$
	$\theta_0 = 114.4$
Dihedral angle CH_2–CH_2–CH_2–*SH*	$a_1 = 5.9046$
	$a_2 = -1.134$
	$a_3 = 13.1608$
Dihedral angle CH_2–CH_2–CH_2–CH_x	$a_1 = 5.9046$
	$a_2 = -1.134$
	$a_3 = 13.1608$

Distance terms inÅ, angles in degrees and energy in kJ/mol.

Table 2. Lennard–Jones parameters for standard non-bonded interactions [17].

	ϵ *(kJ/mol)*	σ *(Å)*
CH_3	0.9478	3.930
CH_2	0.3908	3.930
SH	1.6629	4.450
Au	3.2288	2.737

The parameters found in equations (3) and (4), are given in table 1. Standard non-bonded interactions were modelled with Lennard–Jones 12–6 potentials [23]. These parameters can be found in table 2.

2.2 Spherically averaged gold core nanoparticle

In this section, we discuss the derivation of our spherically averaged model for the gold nanoparticles. The average energy of interaction between a single pseudoatom (SH, CH_2 and CH_3) and the Au_{140} cluster was computed for a given distance, d (the distance from the centre of the cluster to the pseudoatom). The pseudoatom coordinates were randomly generated on the surface of a sphere of radius, d, centred about the cluster. Typically, 10^4 independent configurations were used to obtain the average interaction energy. A full pseudoatom–gold potential energy curve was obtained by systematic calculations at varying radial distances. The resulting potential energy curves were fitted to a modified m–n potential given by,

$$U(r) = 4\epsilon\left[\left(\frac{\sigma}{r - r_0}\right)^m - \left(\frac{\sigma}{r - r_0}\right)^n\right] \quad (5)$$

The r_0 values were subsequently changed to adjust the diameter of the core and hence better reproduce the surfactant density found on the realistic nanoparticle (see next section). The values in table 3 represent the final configuration of the potentials.

2.3 Surfactant adsorption on gold nanoparticles

The Au_{140} passivated nanoparticle was prepared using a method similar to that employed by Luedtke and Landman [10]. The Au_{140} nanocrystal was allowed to equilibrate within a solution of butanethiol molecules for 1 ns (500×10^3 time steps) at 200 K within the NVT ensemble using the Nosé–Hoover thermostat. The temperature was then raised to 500 K in steps of 50 K (20×10^3 time steps each, 20 ps). This allowed for the desorption of excess

Table 3. Parameters for spherical gold core-group interactions (see Eq. (5)).

Group type	m	n	ϵ *(kJ/mol)*	σ *(Å)*	r_0 *(Å)*
CH_3	12	4	2.5033	3.051	5.32
CH_2	12	4	1.6075	3.051	5.32
SH	12	10	581.076	3.43	5.50

butanethiols from the cluster surface and the diffusion of surfactant molecules around adsorption sites. In this way, a compact monolayer of 62 surfactant molecules on the surface of the cluster was generated. The adsorbed thiols formed a hexagonal close packed structure in agreement with the work of Luedtke and Landman [10]. Surfactants found not to be adsorbed were removed and the remaining nanocrystal and surfactants further equilibrated. The dodecanethiol passivated nanoparticle was generated by extension of the surfactant chains. To avoid the trapping of surfactants in non-equilibrium conformations this new structure was simulated at 500 K for 100 ps (50×10^3 time steps) before being slowly relaxed to 300 K in steps of 50 K (50×10^3 time steps).

The model spherical gold nanocrystal was produced in a similar manner. A pseudoatom of gold was grown in a solution of butanethiol molecules to a diameter of 14 Å, over 1 ns (500×10^3 time steps) at 200 K within the NVT ensemble using the Nosé–Hoover thermostat. As previously, the temperature was raised to 500 K in steps of 50 K (20×10^3 time steps each, 20 ps). Again, a compact monolayer of 62 surfactants was formed. The dodecanethiol passivated nanoparticle was generated by extension of the surfactant chains. The r_0 parameter in the fitted potentials was adjusted to better replicate the positional order of surfactants on the realistic cluster. The final configuration of the potentials can be found in table 3.

Typically, the surface density per molecule on planar gold surfaces is 21.4 and 20.6 Å^2 on Au(1 1 1) and Au(1 0 0), respectively. Estimates reveal the sulphur packing density to be around 50% higher on gold crystallites than on planar Au(1 1 1) surfaces [11]. Pradeep and Sandhyarani state a surface density of 15.4 Å^2 molecule [29]. The area per surfactant for our spherically averaged model is 15.1 Å^2, agreeing favourably with both of these estimates.

Noticeably, the spherically averaged model includes no potential for the interaction between different cores. This was determined later through mean force measurements (see next section) and allowed for a separate examination of the nature and influence of the core–core interaction. This spherical model is far less computationally demanding than the real one. We will see below that the properties obtained from the spherical model are in very good agreement with those obtained using the full atomic model.

2.4 Measurement of nanoparticle size and shape

By convention the structure of three and two dimensional lattices of nanoparticles can be rationalised as a packing problem of deformable or compressible spheres [12,19]. Typically, the hardness or softness of passivated nanoparticles has been related to the ratio of the surfactant length to the core radius. Here we examine the size and shape of the nanoparticles at 300 K in vacuum to reveal possible dependencies of size and shape upon the surfactant length and core geometry.

Consider a cluster consisting of n atoms. The centre of this cluster is defined such that $\sum_{i=1}^{n} s_i = 0$, where $s_i = \mathrm{col}(x_i; y_i; z_i)$ is the position of atom i in a frame of reference with its origin at the centre of mass. The radius of gyration tensor, **S**, can then be calculated from

$$\mathbf{S} = \frac{1}{n}\sum_{i=1}^{n} s_i s_i^T = \begin{pmatrix} S_{xx} & S_{xy} & S_{xz} \\ S_{xy} & S_{yy} & S_{yz} \\ S_{xz} & S_{yz} & S_{zz} \end{pmatrix} \tag{6}$$

The tensor, **S**, can be diagonalised to form a diagonal matrix with the eigenvalues L_1^2, L_2^2, L_3^2,

$$\mathbf{S} = \mathrm{diag}(L_1^2, L_2^2 L_3^2) \tag{7}$$

where $L_1^2 \leq L_2^2 \leq L_3^2$. The squared radius of gyration,

$$s^2 = L_1^2 + L_2^2 + L_3^2 \tag{8}$$

provides a measure of the average size of a given conformation, and in this case provides the diameter of the nanoparticle. The asphericity of a given conformation, $\langle A \rangle$, may be defined as [30],

$$\langle A \rangle = \left\langle \frac{\sum_{i>j}^{3} (L_i^2 - L_j^2)^2}{2\sum_{i=1}^{3} L_i^2} \right\rangle \quad \langle A \rangle \geq 0 \tag{9}$$

In practice, for a single nanoparticle 10^7 configurations were sampled with matrix elements being accumulated and averaged before diagonalization of the matrix.

For spherical objects and shapes of high symmetry $\langle A \rangle$ tends to zero, whereas for very elongated objects the asphericity converges to 1. Typical values of the asphericity for ellipsoids with a ratio of major to minor axes of ≈ 1.5 are of the order of 0.1.

2.5 Determination of inter-nanoparticle forces

One objective of the present work is to investigate the effect that core geometry has on the nanoparticle–nanoparticle interactions. With this aim we have computed the mean force acting between the centres of mass of the two nanoparticles at varying distances. Calculations of the mean force have by convention been used to acquire molecular scale knowledge of the solvation forces of particles in solution [31,32].

The mean force is defined as,

$$F(r) = -\frac{dW(r)}{dr} \tag{10}$$

where $W(r)$ represents the interaction free energy between particles. The mean force was computed through constrained molecular dynamics simulations. We considered a single nanoparticle dimer in vacuum with constrained core–core distance, r. Both the dimer and the individual nanoparticles were free to rotate. The surfactant chains were also free to move and adopt favourable conformations. In this way equilibrium configurations were sampled for each interparticle separation, r.

The mean force was computed from,

$$\Delta F(r) = \frac{1}{2}\langle r_u \cdot (F_A - F_B)\rangle \qquad (11)$$

where the brackets indicate an ensemble average; r_u is the unit vector along the core–core constraint bond, and F_A represents the sum of all forces acting upon the core of nanoparticle A. Simulation times of the order of 400–800 ps (4×10^5 and 8×10^5 time steps for butanethiol and dodecanethiol passivated nanoparticles, respectively) were considered to compute ensemble averages. Mean force calculations were performed for both the realistic and model nanoparticles. In order to compute nanoparticle–nanoparticle interactions we employed a cutoff of SOA. The same cutoff was used in the simulations of the two dimensional nanoparticle arrays (see below).

Our spherically averaged model contains no potential to describe the interaction between spherical cores. It has been stated that the dominant contribution to the interparticle potential energy originates from the passivating chains and that the gold core–core interaction contributes only weakly to the overall interparticle energy [11]. To estimate the size of the core–core interaction to the overall mean force, calculations were performed on Au_{140} dimers isolated in vacuum. Such an approach allows the investigation of both the structural and energetic contribution of the gold core to the overall interparticle interaction. The mean force acting on both crystals was recorded for varying separations of the centres of mass. The interaction between gold atoms on different nanocrystals was described by the Sutton–Chen potential [20]. To include all possible orientations the Au_{140} nanocrystals were randomly rotated (10^5 configurations) around their respective centres of mass using a quaternion algorithm [26]. All the simulations were performed using the DLPOLY code [25].

3. Results and discussion

3.1 Structural analysis and melting curves of model gold nanoparticles

A visual analysis of the realistic and model nanoparticles reveals the hexagonal close packed conformation adopted by the sulphur pseudoatoms on both the atomic and the spherically averaged cores (cf. figure 1). In line with previous studies by Landman and coworkers [11], the sulphur pseudoatoms adopt well-defined adsorption sites on both the faces and vertices of the crystalline core. The small size of the crystalline core means that edges and corners form a significant part of the total surface area. This brings about a less than uniform distribution of sulphur atoms as distances between the neighbouring sulphur pseudoatoms vary. For the spherical core the sulphur pseudoatoms are able to form a perfect hexagonal closed packed structure. This difference is best revealed through examination of the pair distribution functions (figure 2) for the isolated nanoparticles. Despite this difference the general similarity of the SH–SH pair distribution functions for both the real and model particles shows that the positional order of the chains is well reproduced by the configured potentials. A comparison of the CH_3–CH_3, CH_3–CH_2 and CH_2–CH_2 distribution functions also show these to be equivalent in both cases (figure 3). This demonstrates that the model closely reproduces the structure of the hydrocarbon chains, suggesting that the difference in core geometry has not altered the structure of the surfactant monolayer.

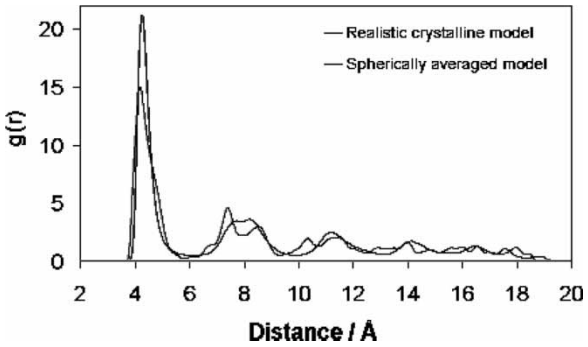

Figure 2. SH–SH pair distribution function for both the realistic crystalline core nanoparticle and the spherically averaged core model.

Examination of the surfactant dihedral angle distributions show that in both the atomic and spherical cores the conformations of the surfactant chains are predominantly trans as has been found for similar particles in both computer simulations [11] and experimental studies [27]. Figure 4 shows the variation in the percentage of trans dihedral bonds as the nanoparticles are slowly cooled from 500 K in steps of 50 K. Though the model appears to slightly underestimate the number of dihedral bonds at very low temperatures there is little or no difference above 200 K. The variation in the percentage of trans dihedral bonds can be used to estimate the melting temperature. According to our results there is no evidence of a clear dependence of the hydrocarbon melting temperatures with core structure.

Figure 5 shows projections of the carbon atom density profiles for the isolated nanoparticles at 300 K in vacuum. The plots clearly show that the time averaged shape (4000 configurations over 5 ns) of all the nanoparticles is approximately spherical. Whilst the model nanoparticles are almost completely spherical, the crystalline core exerts a very small influence over the overall shape of the nanoparticle (cf. table 4). The radius of gyration provides a measure of the particle radius. The extended lengths of the butanethiol and dodecanethiol surfactants are approximately 6 and 16 Å, respectively. This large difference in length is not reflected within their respective radii. This indicates that the dodecanethiol molecules are not to be found in extended conformations despite the high number of trans bonds.

3.2 Mean Force interactions between nanoparticles

The mean force of interaction between butanethiol passivated nanoparticles is shown in figure 6A. The force curve for the spherically averaged core also includes the

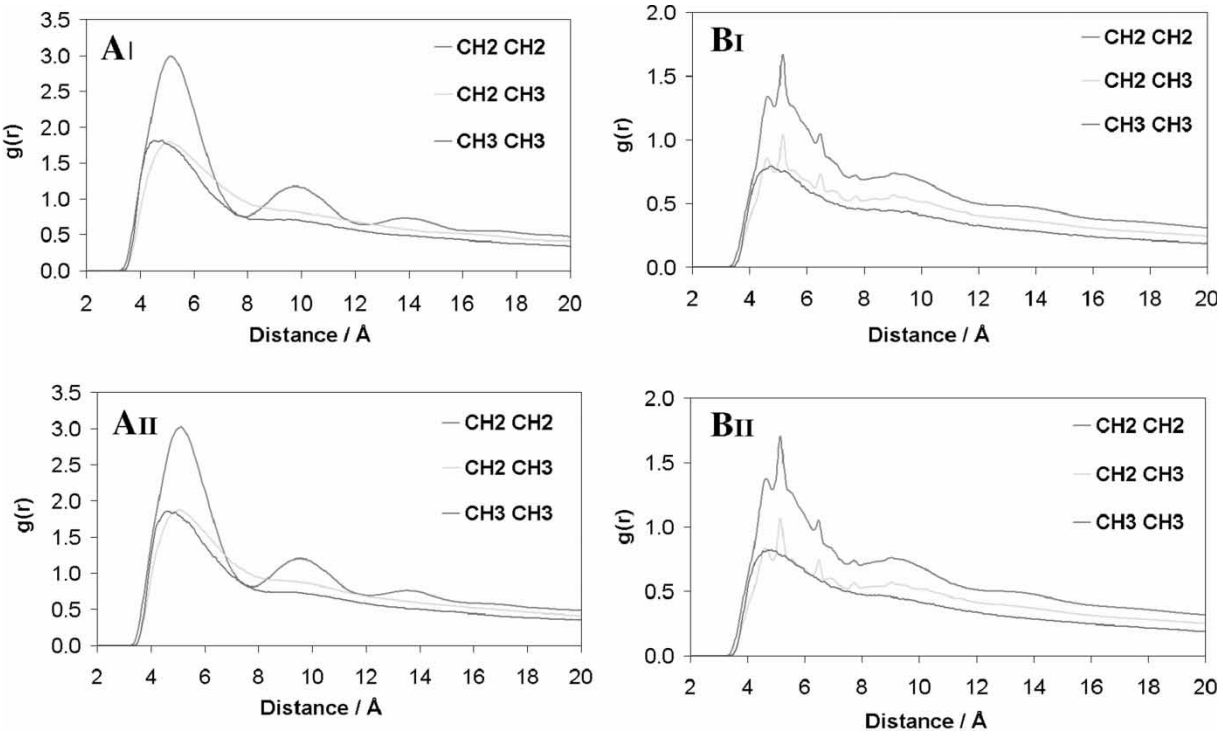

Figure 3. Pair distribution functions describing the structure of the surfactant monolayer for the realistic and model butanethiol (AI and AII, respectively) and for the realistic and model dodecanethiol.

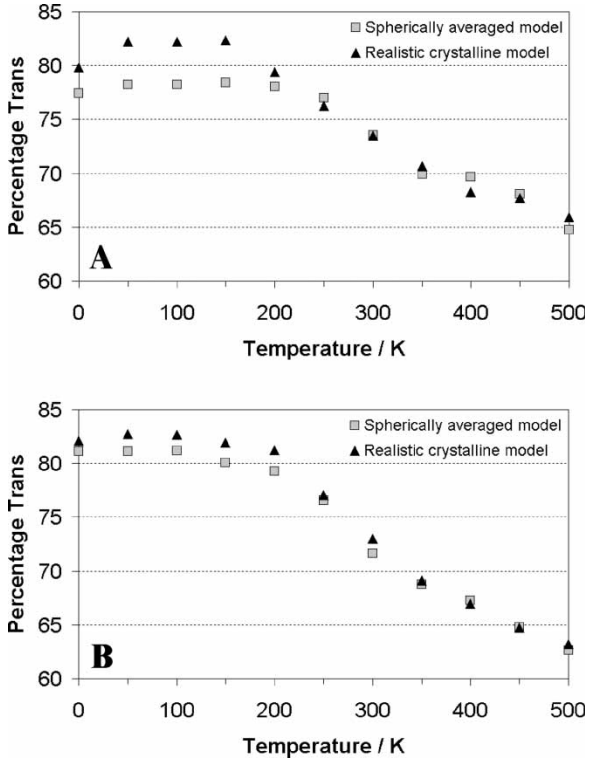

Figure 4. Variation of percentage trans conformations with temperature for both the butanethiol (A) and dodecanethiol (B) passivated nanoparticles with temperature.

core–core interaction determined by simulation of the nanocrystal dimer in vacuum. The two curves for the realistic crystalline and spherically averaged model are remarkably similar with the only differences occurring at distances close to equilibrium which may reflect the different geometry of the cores. The position of zero force, corresponding to the equilibrium separation, is around 23 Å for the realistic dimer and 24 Å for the spherically averaged model. The range of the interaction is noticeably short, effectively zero at 40 Å (approximately twice the size of the diameter of the nanoparticles) in both cases.

The mean force interaction for the dodecanethiol passivated nanoparticles extends over a larger range (figure 6B). Here too the two models are in good agreement. It is proposed that the oscillations in the force curve are linked to the structural changes between opposing hydrocarbon chains. As the two particles approach the surfactant chains are squashed out of the intervening space and in the process slide over one another bringing about oscillations in the force. This is in opposition to the conventional picture of nanoparticle interaction, within the literature, that describes the interdigitaion of surfactant molecules [12]. The equilibrium separation is close to 24 Å in both spherical and crystalline cores. These results indicate that the interparticle forces for both the butanethiol and dodecanethiol passivated nanoparticles are not significantly affected by the core geometry.

Figure 6C shows the mean force curves for the spherically averaged nanoparticles (without the core–core interaction) and also includes the mean force interaction

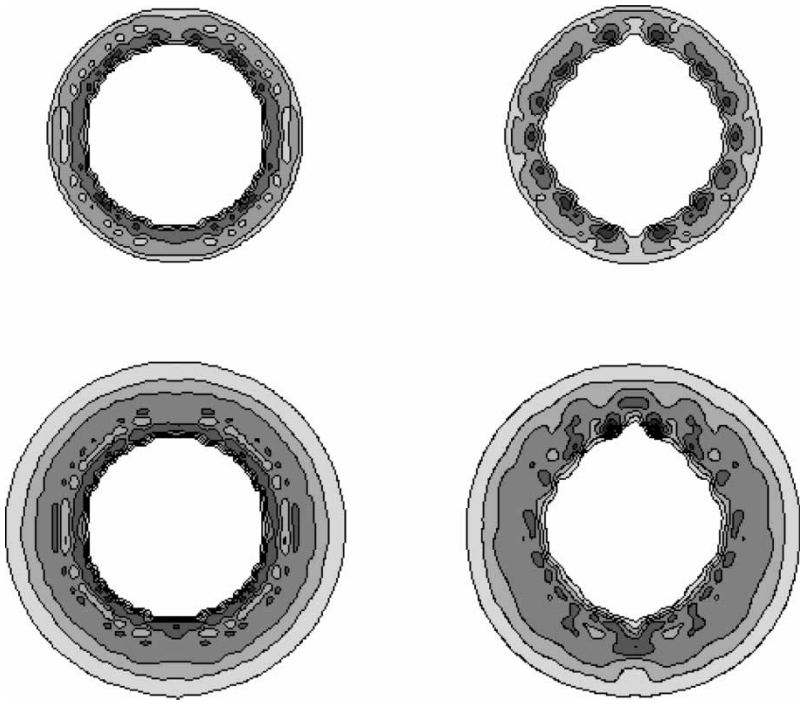

Figure 5. Density plot of carbon pseudoatoms for butanethiol (top left, spherically averaged model; top right, realistic crystalline core model) and dodecanethiol (bottom left, spherically averaged model; bottom right, realistic crystalline core model) passivated nanoparticles.

between two crystalline cores. The very short range of the core–core interaction confirms the fact that it contributes very little to the overall interaction between nanoparticles. At distances above a separation of 26 Å the force between the two crystallites is negligible. This justifies the approximation made in deriving the spherical model, where we neglected to a first approximation the core–core interactions.

Figure 7 shows the potential of mean force (per dimer) of the realistic butanethiol and dodecanethiol passivated nanoparticles as determined by integration of equation (10). The seemingly weak dependence of the equilibrium distance on the surfactant chain length is particularly surprising. For the butanethiol passivated nanoparticle the equilibrium separation lies at 23 Å, whilst for the dodecanethiol passivated nanoparticle the equilibrium separation is 25 Å. The potential of mean force clearly highlights the difference in the interaction range between the short and long chain nanoparticles; though in both cases the range is short in comparison to the diameter of the particles. Also clear is the difference in interaction energy. The far greater interaction of dodecanethiol passivated nanoparticle is expected because of the greater number of interactions between surfactant monolayers. For the butanethiol passivated nanoparticle the equilibrium interaction energy is of the order 130 kJ/mole of dimer. For the dodecanethiol passivated nanoparticle this pair energy is around 315 kJ/mole of dimer. Such values are of the same order of magnitude as a covalent bond. This should have important consequences for the phase stability of the nanoparticle arrays. For instance, the interaction energy in Argon, which is of the order of 1 kJ/mol, results in a triple point temperature of 74 K. If the phase diagram of the nanoparticle arrays would follow a corresponding states law compatible with the phase diagram of Argon, the triple point temperature of the C_4 nanoparticles would be of the order of 5×10^3 K. According to this, gold nanoparticles would always tend to form solid crystal structures at room temperature. This would certainly be the case if other factors, such as the kinetics of self assembly, would not play a role. We will see below that the self assembled structures of C_4 nanoparticles can depart significantly from the expected close packed crystal structure.

Table 4. Asphericity and radius of gyration for butanethiol and dodecanethiol passivated nanoparticles.

C_n	*Type*	*Asphericity*	*Radius of gyration (Å)*
C_4	Model	2.80×10^{-7}	11.9
C_4	Real	0.00013	10.5
C_{12}	Model	0.00014	15.3
C_{12}	Real	0.00033	14.2

Figure 8 shows the carbon atom density around the realistic dodecanethiol passivated nanoparticle dimer at different separations. The equilibrium distance (24 Å) is far too close to allow the interpenetration of surfactants but close enough to yield very strong dispersive interactions between the compressed surfactant monolayers. The shape of the nanoparticles is clearly deformable and two approaching nanoparticles can be seen to induce deformity in one another.

In addition to the constrained molecular dynamics simulation of the nanoparticle–nanoparticle dimer we performed unconstrained simulations of the crystalline

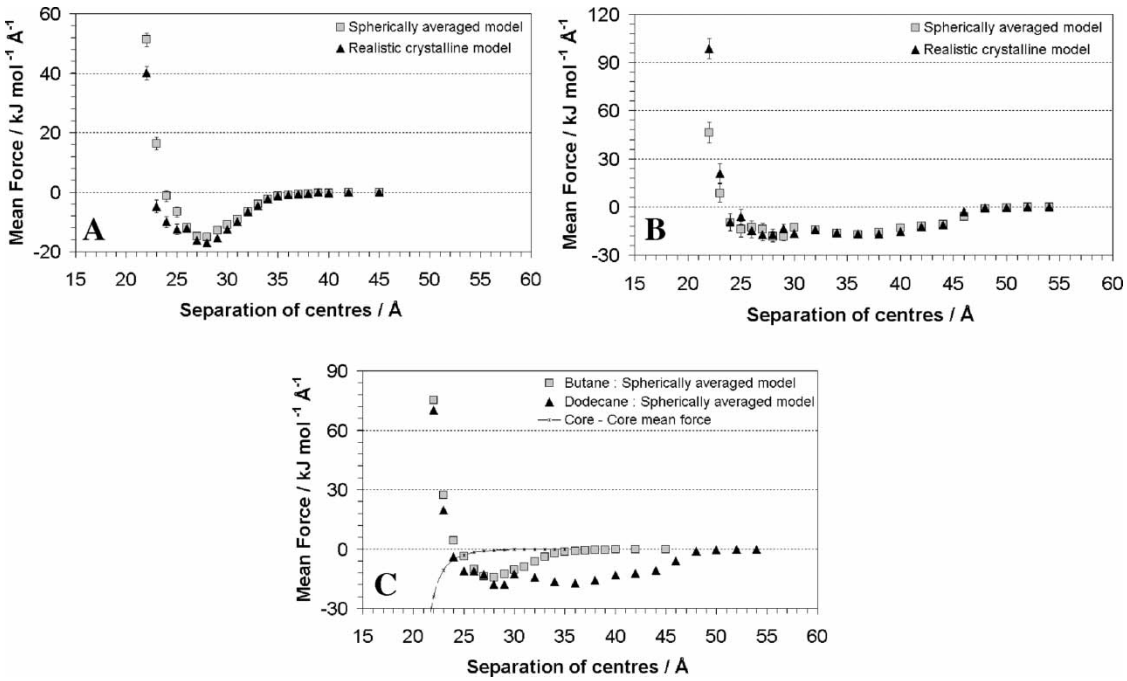

Figure 6. (A) Mean force curves for butanethiol passivated nanoparticles.(B) Mean force curves for dodecanethiol passivated nanoparticles. Both curves for the spherically averaged core model include the mean force contribution from the calculated core–core interaction. Errors are determined from repeated simulations. (C) Mean force curves for the butanethiol and dodecanethiol spherically averaged models (not including the core–core interaction), and the core–core mean force interaction.

core dimmers at 250, 300 and 350 K in vacuum. This study was done to assess the possible effect of the constraint simulation algorithm in determining the nanocluster pair equilibrium configuration. Figure 9 shows the variation of interparticle distance with time. We observe that the unconstrained method results in a nanoparticle equilibrium distance in excellent agreement with the constrained simulations. It is found that the equilibrium distance for both the butanethiol and dodecanethiol nanoparticles is essentially unaffected by the changes in temperature within the range of 250–350 K.

3.3 Simulations of two dimensional nanoparticle arrays

In this section, we discuss computer simulation studies of two dimensional gold nanoparticle arrays. These simulations were performed in vacuum at 298 K in the canonical ensemble. To accelerate the dynamics of the nanoparticles the mass of the gold atoms was set to 10% of its normal value. All movements of the nanoparticles were confined to a plane. With this setup we have investigated the self assembly of gold nanoparticles in two dimensions. This situation is relevant to the aggregation of nanoparticles on solid surfaces and at liquid–vapour interfaces [33]. In the latter case, there have been a number of papers detailing the self assembly of complex structures by nanoparticles adsorbed at air–water interfaces [35]. It has been proposed that the physical origin of these structures is the interpenetration of ligand shells between neighbouring nanoparticles [34]. Computer simulations are particularly useful in studying these systems because they collect direct information on both the surfactant conformations, and the array structure.

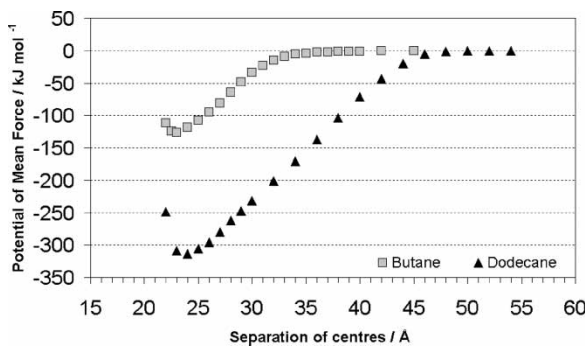

Figure 7. Potential of mean force, per dimer, for the realistic butanethiol and dodecanethiol passivated nanoparticles.

Figure 10 shows representative starting and final configurations of two dimensional arrays involving 64 butanethiol passivated nanoparticles. Starting configurations were formed from square lattice arrangements of the nanoparticles. The butanethiol passivated nanoparticles were found to form an open structure resembling aggregates observed in experiments with silica nanoparticles [28]. These fractal like structures are typical in colloidal systems involving strong interactions. In such conditions the movement of particles is severely restricted preventing the formation of low energy compact structures. This is characteristic of kinetic aggregation processes which produce open, tenuous assemblies. Again, the geometry of the core appears to have little or no influence on the structure of the aggregates, emphasizing the insensitivity of the self-assembly process to the core geometry of the nanoparticles investigated here. In both cases, real and spherical core particle, the nearest neighbour distance is 23–24 Å agreeing

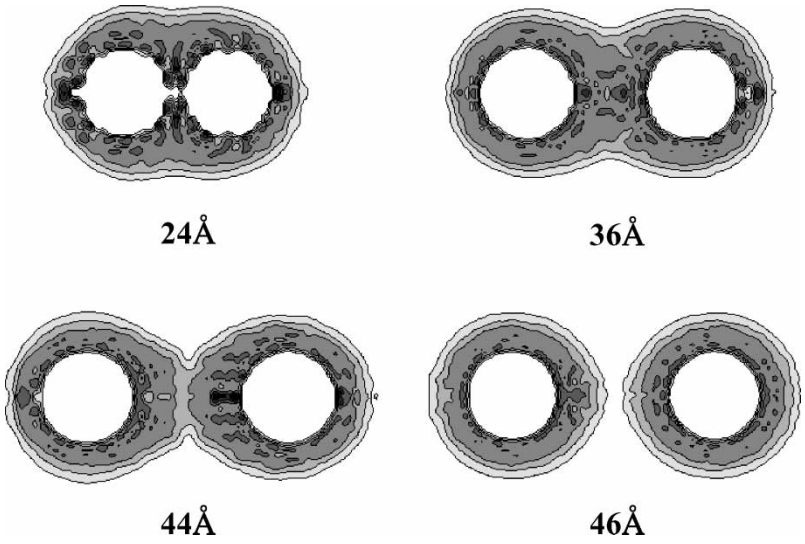

Figure 8. Carbon pseudoatom (CH_2 and CH_3) density plots for nanoparticle dimers (realistic crystalline core model) at different separations.

with the equilibrium distance obtained from mean force calculations of the nanoparticle pair. At this distance the spacing between cores is approximately 6 Å. This is the length of a single butanethiol surfactant molecule and is in good agreement with experimental structural parameters for gold nanoparticle superlattices [19]. The authors note that no preferred orientations of the crystalline clusters were observed, unlike what has been proposed in similar silver nanoparticle three dimensional systems [13]. Our observation seems to be in agreement with experiments of gold nanoparticle arrays performed by different authors [15].

It can be seen from figure 10 that whilst the array is open and tenuous, there are regions of close packing. Figure 11 shows the results of a similar but smaller arrangement of nine butanethiol passivated nanoparticles with crystalline core which formed a hexagonal close packed structure with internanoparticle distances of 23–24 Å. No preferred orientation of the crystalline cores is observed.

The structures formed by the dodecanethiol nanoparticle arrays prove to be more compact but less ordered (figure 12). The nearest neighbour distance for the spherically averaged model is 26–27 Å. For the crystalline core nanoparticles it is a little longer at 27–28 Å. These distances are larger than those obtained by the mean force calculations, suggesting that multiple particle correlations might be important in determining the final structure of the assembly. The presence of neighbouring nanoparticles may prevent the closer approach of two particles through restriction of surfactant conformations. An interparticle distance of 27 Å corresponds to a spacing between cores of roughly 10 Å. This is far less than twice the surfactant length. In three dimensional superlattices of similar particles a spacing of roughly 16 Å has been measured [19]. These smaller than expected particle separations have generally always been attributed to interdigitation [36].

Previous investigations of gold nanocluster arrays in three dimensions have found that the hydrocarbon chain is the most important variable determining the array structure. In our case we find that butanethiol particles are able to form hexagonal closed packed arrays, whereas dodecanethiol nanoparticles form a structure intermediate between a hexagonal close packed structure and a distorted square lattice. It has been observed in experiments of 3D arrays that the fcc structure is observed whenever the ratio of the surfactant length to the core radius, ξ, is smaller than 0.7 [19]. For ratios above this one,

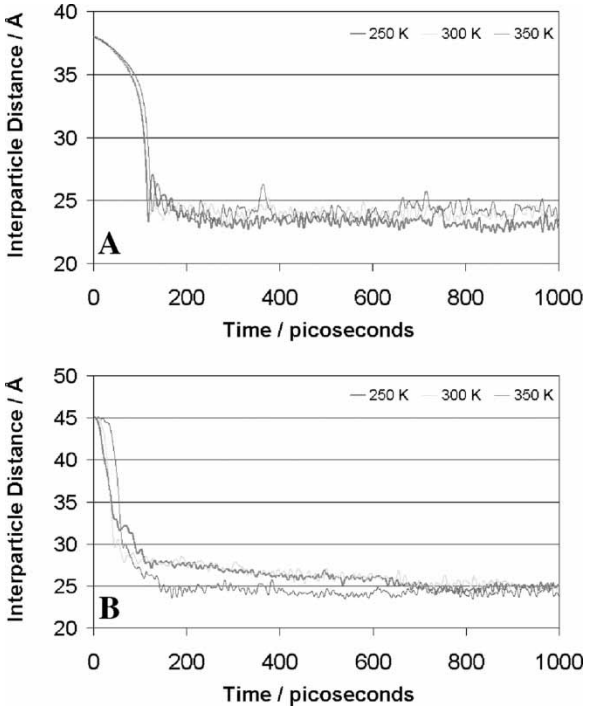

Figure 9. Variation of interparticle distance with time at different temperatures for a single unconstrained dimer of butanethiol (A) and dodecanethiol (B) passivated nanoparticles (realistic crystalline core model).

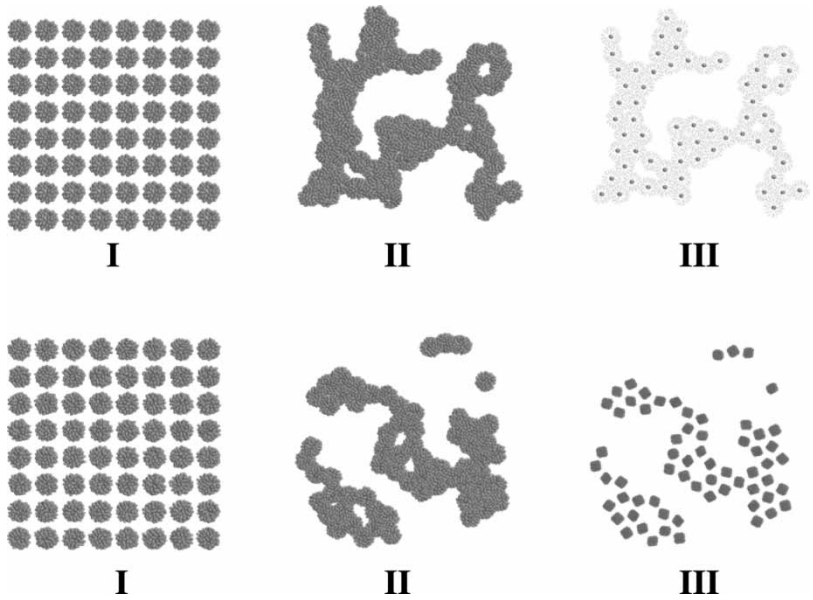

Figure 10. Initial and final configurations of an 8 × 8 array of butanethiol passivated nanoparticles (top, spherically averaged core model; bottom, realistic crystalline core model). Final configurations occur after 0.4 ns.

body centred cubic structures are observed. Landman and Luedtke have observed similar behaviour using molecular dynamics simulations of three dimensional arrays [18]. Our results are in agreement with these experimental and simulation studies. In our case since the array is two dimensional, we obtain hexagonal packing for the butanethiol particles, $\xi = 0.6$, and we get a distorted square lattice for the dodecanethiol systems, $\xi = 1.8$. Simulation studies using our spherical gold core models lead to the same conclusions. This suggests that at least for these small cores the core structure does not determine to a large extent the structure of the clusters. Our results indicate that this is mainly determined by the surfactant chain length (or rather the ratio of the surfactant length to the core radius). The insensitivity of the array structure to the core geometry could be an indication of the lack of orientational correlations between the gold cores in the two dimensional array.

4. Summary and final remarks

We have investigated via molecular dynamics computer simulations, the influence of the core geometry in determining a number of properties of gold passivated nanoparticles; surfactant geometry, surfactants melting temperature, nanoparticle–nanoparticle interactions and structure of two dimensional nanoparticle arrays. We have performed these studies considering a prototypical nanoparticle core, consisting of 140 atoms and surfactants with varying length, C_4 and C_{12}. To address the effect of the core geometry on the properties listed above we have derived a spherically averaged pair potential that models the gold core as a spherical pseudoatom.

One conclusion of this study is that the structure of the gold core, Au_{140}, spherical or polyhedral has little influence on the overall nanoparticle shape, and nanoparticle–nanoparticle interactions. Our simulations of two dimensional arrays using realistic polyhedral cores and spherical cores indicate that the core has not influence on the symmetry of the self-assembled structure either. Indeed we do not find evidence for strong orientational correlations between nanoparticles. These observations can be of relevance to molecular electronic processes, where molecule orientation is an important variable. It should be noted that the conclusions outlined above, may only be strictly valid for the type of nanoparticles

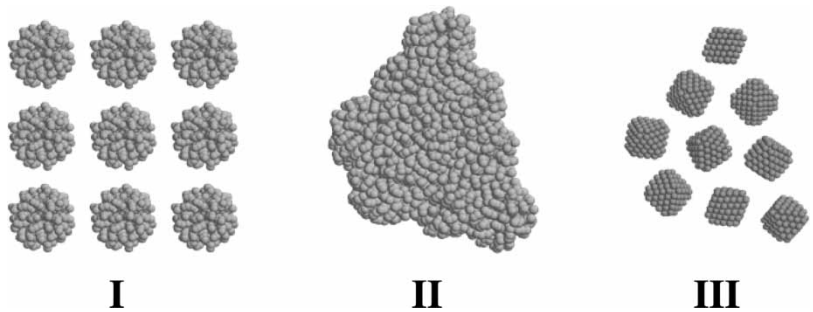

Figure 11. Initial and final configurations of a 3 × 3 array of butanethiol passivated nanoparticles (realistic crystalline core model). Final configurations after 0.4 ns.

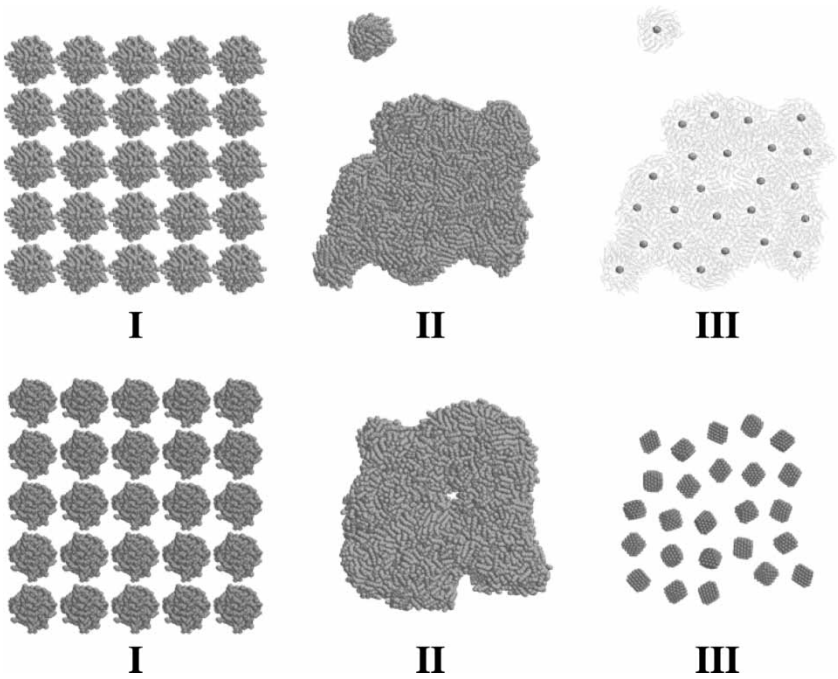

Figure 12. Initial and final configurations of a 5 × 5 array of dodecanethiol passivated nanoparticles (top, spherically averaged core model; bottom, realistic crystalline core model). Final configurations occur after 0.4 ns.

investigated here, i.e. Au_{140} with core diameters of ≈ 1.5 nm. Further work is required to see whether similar observations apply to larger particles. Obviously, we expect that the geometry of the core will become an important factor when the ratio of core diameter to surfactant length is very large.

In addition to the core structure, we have investigated the dependence of the nanoparticle and nanoparticle array properties on the length of the surfactants. The surfactant chains exist in a primarily trans state with gauche defects that increase with temperature to yield more disorder in the chains. We do not find evidence of interdigitation or interpenetration of ligand shells. Indeed, this seems sterically unfavourable and energetically unnecessary as the surfactants can comfortably squash along side one another.

Simulations of short chain surfactant nanoparticles, C_4, in vacuum and in two dimensions, show that nanoparticles then tend to form open cluster structures. This behaviour resembles the irreversible kinetic aggregation observed in other colloidal systems. The physical origin of such structures is a combination of strong nanoparticle attractions and kinetic factors, which prevent the formation of more compact structures in the observation time. Interestingly we find evidence for close packed structures in subdomains within the cluster. Otherwise, long chain surfactant nanoparticles, C_{12}, tend to form more compact clusters consisting of distorted square lattices. The differences between the lattice symmetry observed in the C_4 and C_{12} cases, can be rationalised in terms of the surfactant length to core radius ratio. Our observations in this sense are compatible with previous experiments and simulations of three dimensional structures.

The results reported in this work should be relevant to interpret the behaviour of two dimensional arrays adsorbed at liquid–vapour interfaces. These studies are important to advance in the understanding of the forces operating between nanoparticles adsorbed at fluid interfaces. Progress in this direction requires the inclusion of the solvent. This will enable the investigation of the wetting behaviour of the nanoparticles at the water–air interface. We are at the moment investigating this issue and the results will be reported in a separate publication.

Acknowledgements

This work has been supported by EPSRC Research Grant No. GR/R39726/01. Kafui Tay also acknowledges the award of an MRes in Nanomaterials studentship (EPSRC Research Grant No. GR/R59960/01). Simulations were performed at the HPCx supercomputing center (Edinburgh, UK) under the Materials Chemistry consortium (UK).

References

[1] M.C. Daniel, D. Astruc. Gold nanoparticles: assembly, supramolecular chemistry, quantum-size-related properties, and applications toward biology, catalysis, and nanotechnology. *Chem. Rev.*, **104**, 293 (2004).

[2] F. Bresme, N. Quirke. Computer simulation study of the wetting behavior and line tensions of nanometer size particulates at a liquid–vapor interface. *Phys. Rev. Lett.*, **80**, 3791 (1998).

[3] F. Bresme, N. Quirke. Computer simulation of wetting and drying of spherical particulates at a liquid–vapor interface. *J. Chem. Phys.*, **110**, 3536–3547 (1999).

[4] F. Bresme, N. Quirke. Nanoparticulates at liquid/liquid interfaces. *Phys. Chem. Chem. Phys.*, **1**, 2149–2155 (1999).
[5] F. Bresme. Integral equation study of the surface tension of colloidal-fluid spherical interfaces. *J. Phys. Chem. B*, **106**, 7852–7859 (2002).
[6] J. Faraudo, F. Bresme. Stability of particles adsorbed at liquid/fluid interfaces: shape effects induced by line tension. *J. Chem. Phys.*, **118**, 6518–6528 (2003).
[7] W.G. Gelbart, R.P. Sear, J.R. Heath, S. Chaney. Array formation in nanocolloids: theory and experiment in 2D. *Faraday Discuss.*, **112**, 299–307 (1999).
[8] J. Faradudo, F. Bresme. Anomalous dielectric behavior of water in ionic Newton Black Films. *Phys. Rev. Lett.*, **92**, 236102 (2004).
[9] W.D. Luedtke, U. Landman. Structure and thermodynamics of self-assembled monolayers on gold nanocrystallites. *J. Phys. Chem. B*, **102**, 6566 (1998).
[10] W.D. Luedtke, U. Landman. Structure, dynamics and thermodynamics of passivated gold nanocrystallites and their assemblies. *J. Phys. Chem.*, **100**, 13323 (1996).
[11] J.R. Heath, C.M. Knobler, D.V. Leff. Pressure/Temperature phase diagrams and superlattices of organically functionalized metal nanocrystal monolayers: the influence of particle size, size distribution, and surface passivant. *J. Phys. Chem. B*, **101**, 189 (1997).
[12] S.A. Harfenist, Z.L. Wang, M.M. Alvarez, I. Vezmar, R.L. Whetten. Highly oriented molecular Ag nanocrystal arrays. *J. Phys. Chem.*, **100**, 13904 (1996).
[13] S.I. Stoeva, B.L.V. Prasad, S. Uma, *et al.* Face-centered cubic and hexagonal closed-packed nanocrystal superlattices of gold nanoparticles prepared by different methods. *J. Phys. Chem. B*, **107**, 7441 (2003).
[14] P. Santiago, H.E. Troiani, C. Gutierrez-Wing, J. Ascencio, M.J. Yacaman. Structure and properties of Au nanoparticle superlattices. *Phys. Stat. Sol.*, **230**, 363–370 (2003).
[15] R.L. Whetten, J.T. Khoury, M.M. Alvarez, *et al.* Nanocrystal gold molecules. *Adv. Mater.*, **8**, 428 (1996).
[16] C. Powell, N. Fenwick, F. Bresme, N. Quirke. Wetting of nanoparticles and nanoparticle arrays. *Colloid Surfaces A*, **206**, 241 (2002).
[17] U. Landman, W.D. Luedtke. Small is different: energetic, structural, thermal, and mechanical properties of passivated nanocluster assemblies. *Faraday Discuss.*, **125**, 1 (2004).
[18] R.L. Whetten, M.N. Shafigullin, J.T. Khoury, *et al.* Crystal structures of molecular gold nanocrystal arrays. *Acc. Chem. Res.*, **32**, 397 (1999).
[19] B.D. Todd, R.M. Lynden-Bell. Erratum to "surface and bulk properties of metals modelled with Sutton–Chen potentials". *Surf. Sci.*, **328**, 170 (1995).
[20] B.D. Todd, R.M. Lynden-Bell. Surface and bulk properties of metals modelled with Sutton–Chen potentials. *Surf. Sci.*, **281**, 191 (1993).
[21] H. Sellers, A. Ulman, Y. Shnidman, J.E. Eilers. Structure and binding of alkanethiolates on gold and silver surfaces—implications for self-assembled monolayers. *J. Am. Chem. Soc.*, **115**, 9389 (1993).
[22] T.K. Xia, J. Ouyang, M.W. Ribarsky, U. Landman. Interfacial alkane films. *Phys. Rev. Lett.*, **69**, 1967 (1992).
[23] J.H.R. Clarke, W. Smith, L.V. Woodcock. Short-range effective potentials for ionic fluids. *J. Chem. Phys.*, **84**, 2290 (1986).
[24] T.R. Forester, W. Smith, DLPOLY package of molecular simulation v 2.13, CCLRC, Daresbury Lab. (2001)
[25] M.P. Allen, D.J. Tildesdely. *Computer Simulation of Liquids*, Clarendon Press, Oxford (1997).
[26] A. Badia, R.B. Lennox, L. Reven. A dynamic view of self-assembled monolayers. *Acc. Chem. Res.*, **33**, 475–481 (2000).
[27] M.Y. Lin, H.M. Lindsay, D.A. Weitz, R.C. Ball, R. Klein, P. Meakin. Universality in colloid aggregation. *Nature*, **339**, 360 (1989).
[28] T. Pradeep, N. Sandhyarani. Structure and dynamics of monolayers on planar and cluster surfaces. *Pure Appl. Chem.*, **74**, 1593–1607 (2002).
[29] M. Luo, J. Huang, Y. Chen, J. Xu. Correlation between shape and size of linear polymer chains. *Eur. Polym. J.*, **37**, 1587–1590 (2001).
[30] B.M. Pettitt, P.J. Rossky. Alkali halides in water: ion–solvent correlations and ion–ion potentials of mean force at infinite dilution. *J. Chem. Phys.*, **84**, 5836 (1986).
[31] E. Guardia, R. Rey, J.A. Padro. Potential of mean force by constrained molecular dynamics: a sodium chloride ion-pair in water. *Chem. Phys.*, **155**, 197 (1991).
[32] J.H. Fendler. Nanoparticles at air/water interfaces. *Curr. Opin. Colloid Int.*, **1**, 202 (1996).
[33] W.M. Gelbart, R.P. Sear, J.R. Heath, *et al.* Array formation in nanocolloids: theory and experiment in 2D. *Faraday Discuss.*, **112**, 299 (1999).
[34] R.P. Sear, S.W. Chung, G. Markovich, *et al.* Spontaneous patterning of quantum dots at the air–water interface. *Phys. Rev. E*, **59**, R6255–R6258 (1999).
[35] Z.L. Wang, S.A. Harfenist, R.L. Whetten, J. Bently, N.D. Evans. Bundling and interdigitation of adsorbed thiolate groups in self-assembled nanocrystal superlattices. *J. Phys. Chem. B*, **102**, 3068 (1998).